FUTUREVOLC

European volcanological supersite in Iceland - a monitoring system and network for the future

Report

D8.4: Plume structure and aerosol

Work Package:	*Distribution and description of eruptive products*
Work Package Number :	*8*
Deliverable:	*Plume structure and aerosol*
Deliverable number:	*8.4*
Type of activity:	*RTD*
Responsible activity leader:	*Arve Kylling*
Responsible participant:	*NILU*
Authors:	*Arve Kylling (NILU), Guðmunda María Sigurðardóttir (IMO), Sibylle von Löwis (IMO)*

Type of Deliverable:	*Report*	*[x]*	*Demonstrator*	*[ ]*
	Prototype	*[ ]*	*Other*	*[ ]*
Dissemination level:	*Public*	*[x]*	*Restricted Designated Group*	*[]*
	Prog. Participants (FP7)	*[]*	*Confidential (consortium)*	*[]*

Contents

Summary

Three-dimensional volcanic plume structure may be reconstructed from images of mass column densities obtained from IR and UV cameras. The first part of this report describes the new Iterative Reconstruction of volcanic PLUMes (IRoPLUM) software package which has been developed within the Futurevolc project. IRoPLUM reconstructs volcanic plume structure using the simultaneous iterative reconstruction technique. It has been tested with synthetic data for setups with 3 and 5 cameras. The results show that plume structure may be reconstructed to provide new insight in plume behaviour. The quality of the retrieval increases with increasing number of cameras viewing the same volume. The IRoPLUM software is freely available.

With an Optical Particle Counter (OPC) airborne particle number concentrations and size distributions where measured at different locations in Iceland. The OPC is a commonly used instrument in aerosol research and air pollution studies. The instrument used in this project cover the size range 0.3 to 10 μm particles in diameter. With the knowledge of the particle density a mass eruption rate could be estimated of particles in a certain size range. The second part of this report describes the measurement principle and set-up. During the project a data retrieval mechanism as well as near real time data processing tool was developed. The report shows also some examples of measurements of fine particles during the Holuhraun eruption 2014/2015. The OPC is an easy-to-use instrument which can be rapidly deployed in the vicinity of a volcanic eruption. It can give important information about the size distribution of fine particles within a volcanic ash plume as well as in gas rich eruptions, like in Holuhraun.

1 Tomography

1.1 Introduction

To understand the processes controlling the three-dimensional (3-D) structure of volcanic plumes of ash, sulphur dioxide and other trace gases, methods to derive the 3-D structure of such plumes are needed. The 3-D structure of the volume of interest, is obtained using tomographic reconstruction techniques. Such techniques have been extremely succesful in diagnostic medicine using computer tomography (CT), magnetic resonance imaging (MRI), single-photon emission computed tomography (SPECT), positron emission tomography (PET), and ultrasound scanners. The reconstruction techniques have also found their uses in other areas of science.

Numerous reconstruction methods exists; broadly they may be divided into filtered back projection and iterative algorithms. An overview of the various techniques is given by A. C. Kak and Malcolm Slaney (2001). A short non-technical introduction to image reconstruction is given by Zeng (2001) while Bruyant (2002) gives a sligthly more technical overview. Recent advances in iterative techniques for X-ray CT is presented by Beister et al. (2012).

In medical imaging various back projection algorithms are common due to their computational efficiency. However, the first x-ray computed tomography (CT) scanners used algebraic reconstruction techniques (Wang et al., 2008). Recently there has been increased interest in iterative techniques for computed tomography (Willemink et al., 2013). In geosciences the number of projections may be severely limited compared to medical applications. Also, in medical applications a cylindrical geometry often simplifies the geometry of the problem. The irregularly spaced and limited number of projections, and the non-cylindrical geometry make iterative algorithms the natural choice in geosciences.

The first iterative method was introduced by Gordon et al. (1970) as the Algebraic Reconstruction Technique (ART). ART was used to determine the 3-D structure of individual ribosomes by Bender et al. (1970). It was subsequently shown by Gilbert (1972) that ART in general produces erroneous reconstructions. Gilbert (1972) introduced the Simultaneous Iterative Reconstruction Technique (SIRT) which give superior reconstruction compared with ART. However, SIRT may take many iterations to reach convergence and may thus be computationally demanding. Andersen and Kak (1984) proposed the Simultaneous Algebraic Reconstruction Technique (SART) to remedy this. Generally it is difficult to specify a termination criteria for the iteration technique as convergence depends on the properties of the dataset to be reconstructed (Beister et al., 2012).

ART, SIRT and SART were used by Laepple et al. (2004) for longpath differential optical absorption spectroscopy (DOAS) of NO_2 in a motorway exhaust plume. They found that an improved SIRT gave slightly better results than SART and that ART came off distinctly worse. The first tomography of an SO_2 volcanic gas plume was made by Wright et al. (2008) who used measurements from five scanning spectrometers that viewed a gas plume from Mt. Etna. Johansson et al. (2009) presented further tomographic reconstruction of gas plumes using a variation of the Low Third Derivative (LTD) method proposed by Price et al. (2001). Kazahaya et al. (2008) used a variant of this method for computed tomography reconstrcution of SO_2 concentrations using data from three UV spectrometers on board a helicopter.

The development of UV, visible and infrared (IR) cameras has allowed the retrieval of images of volcanic ash mass and SO_2 (Prata and Bernardo, 2009, 2014). Viewing a volcanic plume from several directions with several cameras placed in a favorable geometry, may allow the 3-D structure of the plume to be reconstructed from the volcanic ash mass or SO_2 images. Within Futurevolc a new software package, Iterative Reconstruction of volcanic PLUMes (IRoPLUM), has been developed for the reconstruction of volcanic plumes from ground based cameras measurements. In this report IRoPLUM is described and synthetic examples of its use are presented. Based on the findings of Laepple et al. (2004) on the reconstruction quality of ART, SIRT and SART, the software implements the SIRT method.

The software is based on the following assumptions:

- The 2-D images of mass loading (slant column densities) covering a 3-D volume, have been rebinned into slices to allow slice-by-slice 2-D reconstruction.

- The reconstruction grid has the same spatial resolution in the horizontal and vertical directions.

- Reconstruction is made for pixels traversed by at least one ray from each camera. Other pixels are set to zero density.
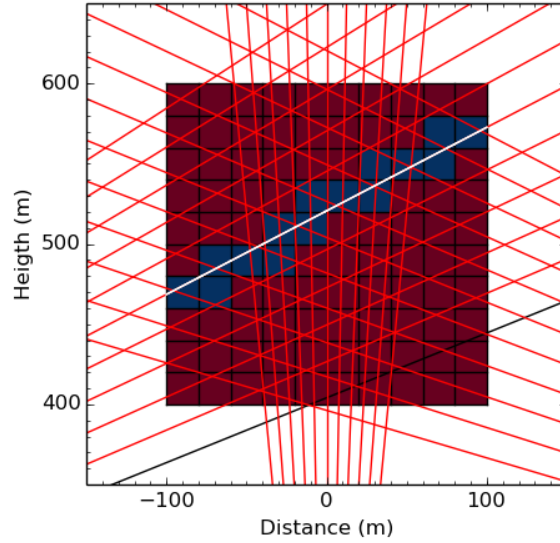
Figure 1: Illustration of rays (viewing directions) for three cameras (see also Fig. 2). The black horizontal and vertical lines indicate the reconstruction grid. Pixels that are traversed by the red and white ray are colored blue. The white part of the ray indicates the part of the ray included in the calculation of the line integral. Note that for a real application the number of rays would typically be much larger and the pixel size similarly much smaller.

- All pixels covered by one ray that has slant column density below a given threshold (default=0.0), are set to zero density.

The rest of the report is structured as follows: in subsection 1.2 SIRT is presented. This is followed by a description of various synthetic phantoms[1] used to test the implementation of the algorithm, subsection 1.3. This subsection also includes a description of the synthetic sinograms[2] calculated from the phantoms for various camera setups. Reconstruction results are presented in subsection 1.4.

1.2 Algebraic Reconstruction

For a set of measured column densities $P_{k\theta}$ we want to reconstruct the density ρ_{ij} in a given plane at each point $(i, j), i = 0, \ldots, n-1; j = 0, \ldots, n-1$, within a square of $n \times n$ points. The pixels are bounded by $n+1$ equally spaced horizontal and vertical lines as shown in Fig. 1. For a given ray k with the projection at angle θ, the total density or line-integral (also called ray-sum by A. C. Kak and Malcolm Slaney, 2001), is

$$R_{k\theta} = \sum_{(i,j) \; \varepsilon \; k\theta} l_{ij}\rho_{ij}. \tag{1}$$

Here, the sum is over all pixels (i, j) traversed by the k'th ray and l_{ij} is the length of the k'th ray in the pixel. Note that the width of the ray is assumed to be negligible. In practice this implies that the resolution of the reconstruction grid must be coarser than the measurement grid. In Fig. 1 the blue pixels are traversed by the white line which represents the part of the ray that is included in the calculation of $R_{k\theta}$.

To reconstruct the density ρ_{ij} from $P_{k\theta}$, we use the Simultaneous Iterative Reconstruction Technique (SIRT, Gilbert, 1972). The iteration is started by assuming a constant density field ρ_{ij}:

$$\rho_{ij}^0 = T/n^2, \qquad i, j = 1, \ldots, n \tag{2}$$

---

[1] A phantom is an artifical object used as a substitute of the real thing. A synthetic phantom is a computer representation of the object.
[2] A sinogram is a visual representation of the raw data obtained in tomography.

where the total density T of the plane is

$$T = \sum_{k=0}^{N_{rays}-1} P_{k\theta},$$ (3)

and N_{rays} is the total number of rays. Note that for a pixels to be included in the sum for T the pixel must traversed by at least one ray from each camera. Also, pixels covered by one ray that has slant column density below a given threshold (default=0.0), are not included. An updated density is obtained from (Eq. (7) Gilbert, 1972)

$$\rho_{ij}^{q+1} = \max\left[\rho_{ij}^q + \frac{\sum P_{k\theta}}{\sum L_{k\theta}} - \frac{\sum R_{k\theta}^q}{\sum L_{k\theta}}, 0\right],$$ (4)

where $L_{k\theta}$ is the length of the ray $R_{k\theta}$. Eq. 4 is the additative implementation of SIRT. There is also a multiplicative SIRT which is not considered here (Gilbert, 1972). The SIRT implemented is standard with exception of the camera geometry. It is noted that for CT scanners, statistical iterative reconstruction is a hot research topic and results from that community may be utilised in geosciences as well (Wang et al., 2008).

In the validation experiments below the reconstructed density field, $\rho_{rec}(r)$, is compared against the "real" (synthetic) density fields, $\rho_{real}(r)$. As a quality criterion for comparison the nearness criterion as defined by Laepple et al. (2004) is used:

$$\text{Nearness} = \frac{1}{N}\sqrt{\int dr^2(\rho_{real}(r) - \rho_{rec}(r))^2}$$ (5)

where

$$N = \sqrt{\int dr^2(\rho_{real}(r) - \overline{\rho_{real}(r)})^2}$$ (6)

A nearness of 0 implies perfect agreement while a nearness of 1 implies that the reconstructed field is the same as the initial constant average field.

1.3 Phantoms and Simulated Sinograms

To test the reconstruction algorithm, synthetic line integrals were constructed for a target plume. The aim of the test was to test the reconstruction of a horizontal ash or SO_2 plume downwind of a volcano for various camera setups. The synthetic line integrals were calculated by the `SyntheticLineIntegrals.py` script from the IRoPLUM package, see Appendix A.

Downwind of a volcanic plume realistic ground based camera positions may be to the side of and below the plume. Such a potential setup is shown in the left plot of Fig. 2. Camera 1 is located 1000 m to the left of the target center. Camera 2 is elevated 100 m relative to camera 1 and views the target from the right. Camera 3 is placed directly below the target. It is noted that the locations of the cameras are idealised. In realistic conditions the plume may be offset with respect to the FOV of the cameras. Hence, for real measurements careful considerations must be made with respect to camera placement and FOV and the most likely position of the plume. The locations of the cameras are summarized in Table 1. Each camera is taken to have 201 pixels in the vertical direction with a field of view (FOV) of 20°. This is different from typical IR cameras [3], but is fully user controllable in the software. More pixels will increase the spatial resolution but should have little impact on the reconstruction of the shape of the plume.

An example of a square reconstruction area is shown in grey in Fig. 2. The target is a mixture of two Gaussian concentrations, blue blurred dots in left plot of Fig. 2. The line integrals for each camera are shown in the right plot of Fig. 2. For camera 1 and 3 the gap between the two Gaussian concentrations is visible in the line integrals. Camera 1 is brighter since it sees the integral of both Gaussian concentrations.

A setup with 5 cameras is shown in Fig. 3. Below SIRT is used to reconstruct the density fields from the sinograms in

---

[3]The NicAIR II cameras used in Futurevolc have 480 pixels in the vertical and a vertical FOV of 27°, http://nicarnicaaviation.com/wp-content/uploads/2014/04/NICAIR2-TECH-DOC.pdf
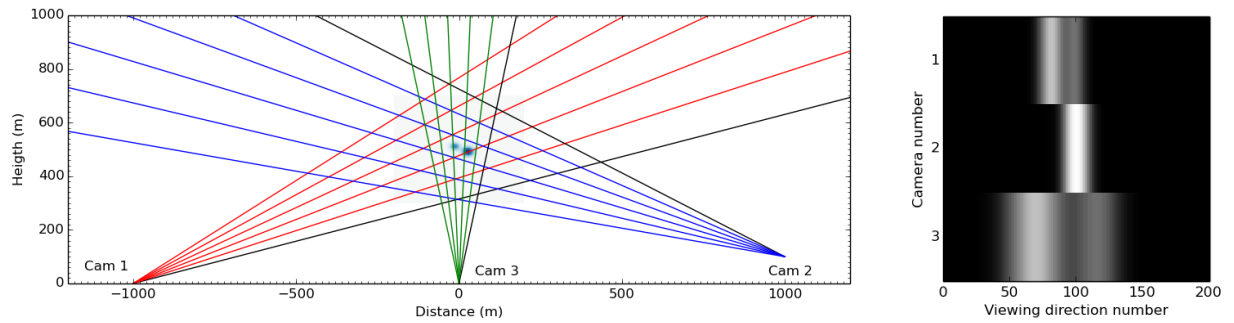
Figure 2: (left) A camera set up with selected viewing directions. The target consists of two Gaussian concentrations with full width half maxima (FWHM) of 25 and 30 m and offset from the center. The maximum of the rightmost (leftmost) Gaussian shape is 1.5 (1.0). The horizontal and vertical resolution (pixel size) is 2.5 m. The rays are in different colours for the different cameras, except for the first ray (smallest viewing angle in Table 1.) which is black. Only a few rays are shown for each camera for clearness. The reconstruction is represented by the gray area. (right) The line integral for each viewing direction for each camera in the left plot.

Table 1: Camera geometry for cameras in Figs. 2 and 3.

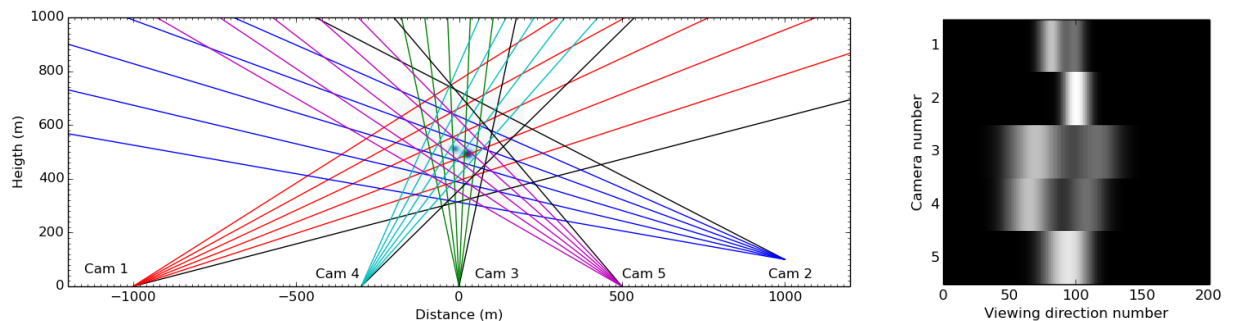| Camera	Location (x,z) (m)	Viewing range (degrees)
1	(-1000,0)	17.5-37.5
2	(1000, 100)	148.0-168.0
3	(0, 0)	80.0-100.0
4	(-440, 0)	50.0-70.0
5	(500, 0)	125.0-145.0

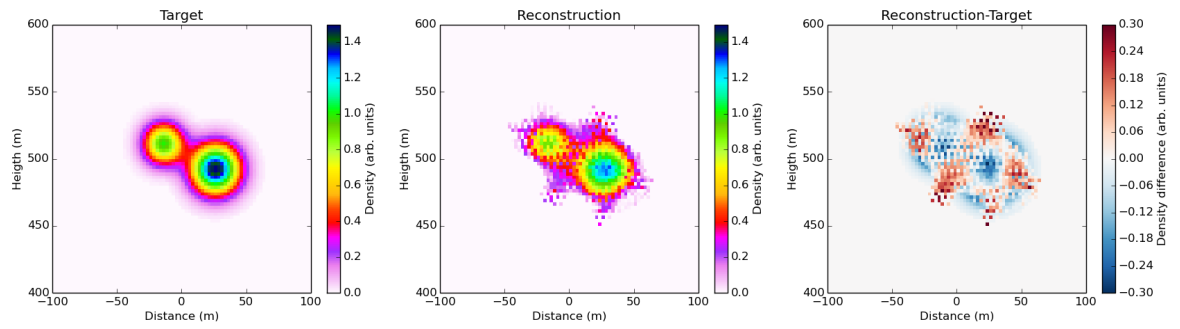Figure 3: Similar to Fig. 2, but with 5 cameras viewing the plume.

Figure 4: (Left) Zoomed in view of the "real" density field in Fig. 2. (Middle) Reconstructed density field using the three cameras set up shown in Fig. 2. (Right) the difference between the "real" and reconstructed density fields.
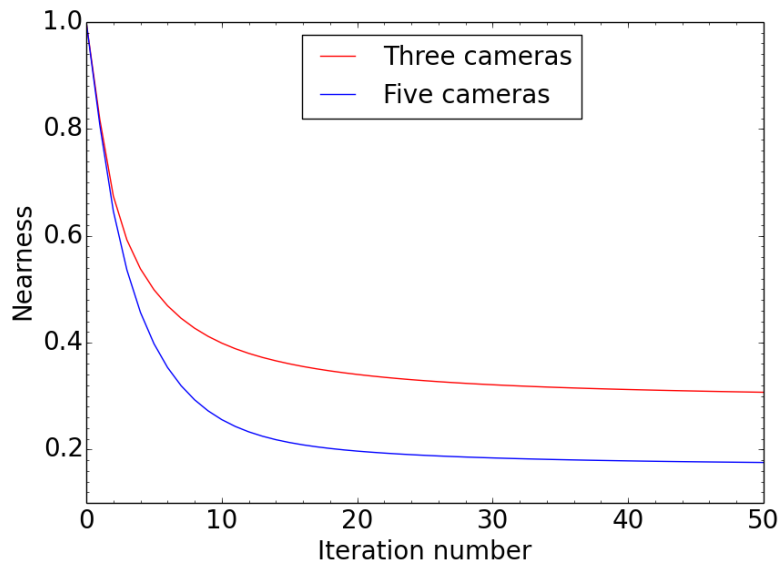

Figure 5: The nearness as a function of iteration number for the reconstructions in Figs. 4 and 6.

Figs. 2 and 3.

1.4   Reconstruction results

A grid of 160×160 pixels centered at $x = 0$ m, $z = 500$ m, with each pixel of size 2.5×2.5 m^2 was used for the reconstruction. The number of iterations was set to $N_q = 50$. In the left plot of Fig. 4 is shown a zoomed in view of the "real" density field in Fig. 2. The reconstructed density field is shown in the middle plot of Fig. 4 and the difference (reconstruction-"real") in the rightmost plot. The nearness is shown as a function of the iteration number in Fig. 5, red curve. The reconstruction reproduces the overall features of the "real" density field. The peak in the density field is underestimated by 14%. The reconstruction also have some isolated low density noise outside the region covered by the "real" density field. These pixels may be filtered out by applying spatial noise-reduction techniques (Francis et al., 2012).

Part of the differences seen in the difference plot in Fig. 4 is caused by the limited number of view angles of the three cameras. More cameras at other angels should improve the results. Various measurement geometries have been evaluated for tomographic reconstruction of air pollutants by Todd and Bhattacharyya (1997) and Hartl et al. (2006). Here, we increase the number of cameras to 5 as shown in Fig. 3. The resulting reconstruction using sinograms from
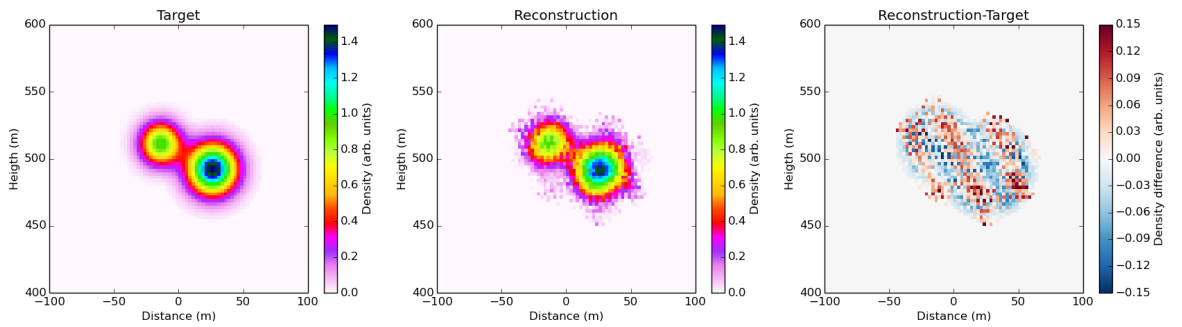
Figure 6: Similar to Fig. 4, but here reconstruction is made using the five cameras set up shown in Fig. 3. Note that the y-axes are different in the rightmost plots in Figs. 4 and 6.

5 cameras is shown in the middle plot of Fig. 6. Compared to the reconstruction in Fig. 4, using data from 3 cameras, the reconstruction with 5 cameras is both qualitatively better by comparing the middle plots in Figs. 4 and 6, and quantitatively by comparing the difference between the "real" and reconstructed densities, right plots Figs. 4 and 6. Also the peak in the density field is for the 5 cameras reconstruction underestimated by 4% compared to 14% for the 3 cameras reconstruction. Finally thee nearness is better for 5 cameras, Fig. 5. From Fig. 5 it is seen that about $N_q = 30$ iterations is sufficient.

It is noted that the sinograms are assumed to contain no noise. Real measurements do contain noise and reconstructions from real measurements may thus be more noisy. The measurement noise may be treated by statistical iterative methods, but that is beyond the scope of the present work.

During volcanic eruptions the deployment of cameras in positions such as to make the measurements amendable to tomography may pose a challenge. However, from the synthetic data presented above a few suggestions may be made:

- Cameras must be place at such a distance that the full plume is in the field-of-view of all cameras.

- Accurate alignment of cameras are required to ensure that pixels (rays) from different cameras may be identified to view the same plume volume.

- Due to the physics involved in deriving the mass loadings, tomography of ash and SO_2 plumes are only possibly in the non-opaque parts of the plumes.

- The plume geometry defines how the cameras should be set up for tomography measurements. For a horizontal plume cameras may be placed on a line perpendicular to the plume direction. For a vertical plume cameras may be placed in a circle surrounding the plume.

- The computational time of the reconstruction depends on the number of camera pixels and the number of cameras. Speed ups are possible to make tomography feasible in a monitoring situation.

1.5   Reconstruction software

The algorithm described above is part of the IRoPLUM software package. IRoPLUM is a collection of python scripts (https://www.python.org/). The content and use of IRoPLUM is described in Appendix A. IRoPLUM is available as free software under the GNU General Public License (http://www.gnu.org/licenses/licenses.html) from http://folk.nilu.no/~arve/.

1.6   Conclusion

The IRoPLUM software package developed as part of the Futurevolc project have been described and tested on synthetic data. Given mass loading (slant column density) measurements of any gas or ash plume from multiple cameras

viewing the same volume of the plume, the 3-D plume structure may be reconstructed by: 1) re-binning the measurements into slices; 2) For each slice IRoPLUM may be used to reconstruct the 2-D structure of the slice; 3) Stacking the slices finally gives the 3-D structure of the plume.

2 Optical Particle Counter (OPC)

2.1 Introduction

In May 2013 the Icelandic Meteorological Office (IMO) started a work on setting up two Optical Particle Counters (OPC) as part of the FutureVolc project. The OPC is a widely used instrument in aerosol research. It rapidly provides information on aerosol size distributions. The device used in our project measures and counts airborne particles in a size range of 0.3 to 10 μm in particle diameter. The aerosol sample flows through a laser beam. From the intensity of the detected scattered light the particle size can be calculated (see subsection 2.2).

In the course of the project, the OPCs were installed at different locations in Iceland, most recently near the eruption site in Holuhraun north of Vatnajökull. The remote communication with the instruments and data streaming were tested, and an automated data processing tool was developed. In the case of a volcanic eruption, the instruments can be quickly installed and data streamed into the FutureVolc database. The OPC measures the aerosol size distributions and number concentrations in a certain size range. With the knowledge of the particles density a mass eruption rate could be estimated of particles in this size range.

This section contains a brief description of the equipment that has been used for the measurements of aerosol particles, its installation and the choice of measurement locations. It also discusses the remote communication with the instrument, configurations and data processing.

2.2 Instruments and Setup

OPC: The instrument used is an Optical Particle Sizer, Model 3330 from TSI Inc. It operates on the principle of single particle counting using a detector to detect particles passing through a sample volume illuminated by a laser beam. Aerosols are drawn into the inlet with the flow rate of 1 L/min. The aerosols are immediately surrounded by a particle free sheath air flow of 1 L/min (picture 1). In the optics chamber the sample flows through a focused laser light beam, where only one particle is illuminated at a time and scatters a pulse of light to the photo detector. The pulse of light is converted to an electrical signal. To interpret the pulse and direct a count to the correct size range, electronic pulse height analysis is used. In each size range or channel, the total counts are accumulated (Hinds, 1999). The OPS 3330 can provide measurements of number concentrations in up to 16 size channels in a particles size range of 0.3-10 μm. Particles larger than 10 μm can be detected and counted but they cannot be size classified. For particles smaller than 0.3 μm the counting efficiency is 50%. After being sized, the sample flow exits the optics chamber and particles are removed by a particle filter. This removable filter that can later be used for chemical analysis and the pump is protected from contamination. The sample flow is then split into two: one half lefts the instrument through an exhaust tube, but the other half circulates in the OPC to maintain the sheath air flow (Model 3330 Optical Particle Sizer Spectrometer, 2001).

Enclosure: TSI DustTrakTM Aerosol Monitor Environmental Enclosure, Model 8535. Designed for TSI's instruments and fits around the OPC. The instrument is fixed in the enclosure and there is enough space for a modem, heating element and possibly a small computer. On top of the enclosure is an air inlet assembly screwed on which is connect to the inlet of the OPC. Water and larger particles are trapped in a water bottle screwed on the inside of the top cap of the enclosure. The enclosure has a DC power connector, USB pass-through connection along with antenna cable strain relief and plug.

The enclosure can be mounted on a tripod to enable measurements well above ground.

Modem: 3G UMTS/HSPA modem UR5i v2 comes with built in router, power supply, crossover UTP cable and external antenna. Standard version of the modem is equipped with one Ethernet 10/100, one USB Host port, one
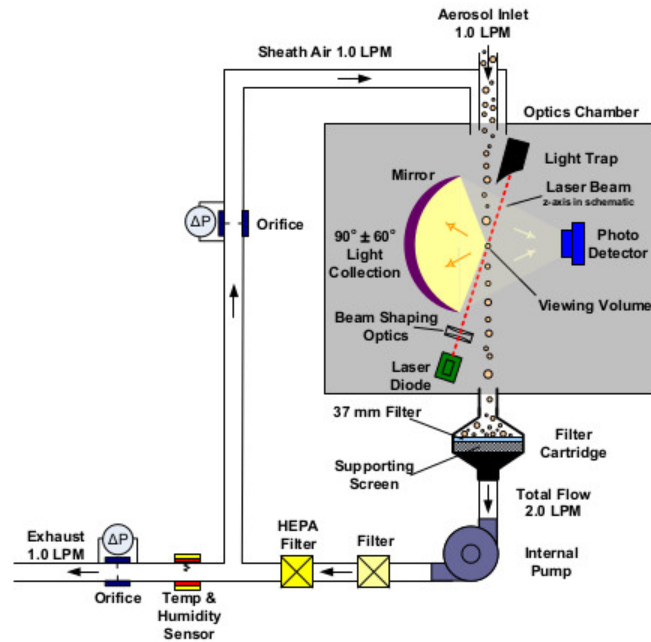
Figure 7: Particles flow path in the OPC (Model 3330 Optical Particle Sizer Spectrometer, 2001).

binary input/output port and one SIM card (possible to have two). The wide range of interface options of the modem further expands Port1 and Port2. Configuration is done via web interface protected by password.

Heating: A heating element (STEGO HGK 047, AC/DC120-240V 10W) is used to protect the OPC from temperatures below zero degrees within the enclosure. The heating element is regulated by a thermostat (STEGO KTO 011, AC120V).

2.3   Configuration

When measuring with the OPC it has most often been scheduled with a sample length of ten minutes and then give total counts of particles in each of the sixteen bins. These ten-minute-measurements are repeated continuously. The smallest particles are most frequent, and the first six size bins represents particles smaller than 1 μm, next four bins are particles 1.2.5 μm and particles 2.5-10 μm are counted in the last 6 bins (Table 2). Number of bins, up to 16, and the setup parameters for each channel are changeable. Channels cannot be set below 0.3 or above 10.0 μm. Channels may not overlap one another and must be continuous. Sample scheduling is flexible, and sample length can be set to one second up to 24 hour.

2.4   Communication, data processing and plotting

Communicating remotely with the OPC was not as easy as initially assumed. The idea was to connect remotely to the OPC through a 3G modem to get saved data files from the OPC. It turned out that it is not possible to empty the instruments memory remotely. Old data are not overwritten. Therefore, the instruments stops measuring when the internal memory is full. Unfortunately the manufacturer's advice could not solve this problem. The manual recommended commands are only for receiving the data and the status of the instrument but not for downloading or deleting. The only solution suggested requires a stop of the measurements for a certain time period. This time period

Table 2: Measured particles of diameter 0.3-10 μm are sized and binned up in 16 channels.

Bin #	Particle diameter (μm)
bin 1	0.3-0.374
bin 2	0.374-0.465
bin 3	0.465-0.579
bin 4	0.579-0.721
bin 5	0.721-0.897
bin 6	0.897-1.117
bin 7	1.117-1.391
bin 8	1.391-1.732
bin 9	1.732-2.156
bin 10	2.156-2.685
bin 11	2.685-3.343
bin 12	3.343-4.162
bin 13	4.162-5.182
bin 14	5.182-6.451
bin 15	6.451-8.031
bin 16	8.031-10

depends on the amount of data to be downloaded and thus, this method is not convenient when monitoring a volcanic eruption.

To communicate with the device and to get data remotely a shell is opened and the instrument accessed via telnet. The instrument can be scheduled and controlled via telnet. It can be started, stopped and shut down, but it can't be turned on remotely. To get real time data from the OPC a script is run via telnet where end values from last measurement are collected.

When measuring over a period of time, the OPC has been scheduled to sample over ten minute intervals. The script is sending commands every 10 minute to get the end value from the last measurement. The script also asks for the time stamp of the OPC and of the computer. The data collected are gathered in to a daily file and a new file is created every day.

Today data collection and presentation from the OPC has been automated on a central server at VÍ. The collection depends on BASH shell script, telnet and internal commands on the instruments. Telnet connection is set up once every 10 minutes over the mobile connection and the instrument queried for last 10 minutes measurement. The results is appended to a file which is generated at the beginning of each day.

The BASH shell script is hosted on a server at IMO home office. The daily files are stored on a dedicated network drive at IMO where they are available to any service needing to process them. The folder tree structure on the file server is based on the date. Each element of the date represents a new folder and the inner most folder is the serial number of the instrument. Thus, the instruments can be separated when measuring simultaneously.

In the folder containing the measurement files, a description file of the metadata, i.e. information about location name, coordinates, the OPC firmware information and result from status commands.

An R script has been written which retrieves data from the file server and compiles figures showing the results from the measurements. The script crawls through the last seven days on the files server collecting all measurements and relevant information from the description file. It gives one figure per location with as many days as available (maximum seven). The figures are overridden with each run which is schedules once per day.

Since the measurements on the file server aren't post processed, the R script has to rely on a bash script doing the post processing. Along with that the R script uses a handful of system functions relying on the Linux operating system running it.

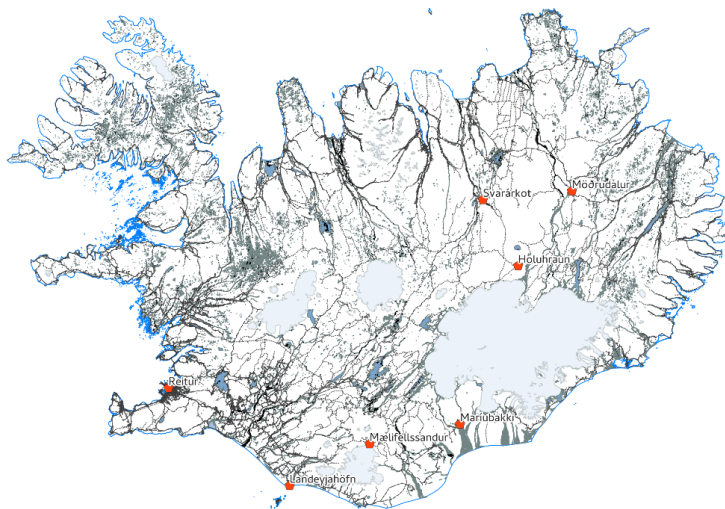Figure 8: a) The OPC is measuring in Möðrudalur in September 2014, and b) Look inside of the enclosure.

Figure 9: Map of Iceland. Red dots are OPC measurement locations in 2013-2014.

2.5   Setup

The environmental enclosure is mounted to a survey tripod. The OPC and the modem is placed inside the enclosure. An antenna is connected to the modem and mounted on top of the enclosure. The sample inlet tubing from the enclosure is connected to the inlet of the OPC. The inlet is screwed to the inlet ring on top of the enclosure. The modem is connected to the OPC with Ethernet cable. Both devices are connected to a rectifier which is passed through the enclosure with AC cable to electricity from the power supply system. The heating element with thermostat was installed in summer 2014 to keep the inside temperature of the enclosure above zero degrees.

During field campaigns the equipment, except for the heating, can be operated on 12V DC through high capacity batteries.

2.6   Measurement locations

The OPC has been measuring at various locations in Iceland in 2013-14 (Fig. 9). At some locations, dust storms or re-suspension of volcanic ash particles have been already observed. Furthermore, the OPC instruments were part of a measurement campaign as well as several volcanic exercises. During the volcanic eruption 2014/2015 in Holuhraun

both instruments were installed at different locations in the near and far field to the eruption site.

2.6.1 Svartárkot

Svartárkot in Bárðardalur in North Iceland was chosen because of its good location in terms of volcanic eruption in Vatnajökull area (Grímsvötn and Bárðarbunga) and Askja, respectively. The sand area in the north of Vatnajökull is a known source of sand and dust storms, which are occasionally observed in Bárðardalur. The soil contains aged volcanic ash from prior eruptions as well as eroded lava fields and other material, e.g. former glaciers (Arnalds et al., 2001).

At Svartárkot the Icelandic Met Office (IMO) operates an automatic weather station which is an advantage when analysing the data from the OPC. To interpret the OPC data it is important to identify the source of the suspended airborne particles. The knowledge of the atmospheric conditions is therefore essential.

The OPC at Svartárkot was installed on 25 June 2013 and taken down 29 August 2013. At that time the heating equipment was not available and the weather forecast predicted cold weather. Therefore, it was decided to take the instrument down. At that time, data couldn't be collected remotely and were only be stored in the instruments internal memory.

2.6.2 Mælifellssandur

In August 2013 the OPC was installed during a measurement campaign in Mælifellssandur in the highlands, north of Mýrdalsjökull. In this area dust storms or dust re-suspension events are frequently observed. The goal of this campaign to measure the particle size distribution and number concentration of dust particles with different instruments during such an event (Dagsson-Waldhauserova et al., 2014).

2.6.3 Maríubakki

Maríubakki is located north of Kirkjubæjarklaustur in Southeast Iceland. Like Svartárkot Maríubakki is close to the volcanoes of the Vatnajökull glacier-Grímsvötn, Bárðarbunga, Gálp as well as the volcano Katla in Mýrdalsjökull glacier. Thus, it is an advantageous location with regard to the measurement of fine particles emitted during volcanic eruptions. It is also well located to measure dust storm events and re-suspended ash from Grímsvötn eruption 2011, respectively.

2.6.4 Landeyjarhöfn

The OPC was up and running in Landeyjarhöfn in South Iceland 21-24 February 2014. Landeyjarhöfn is a harbour located in the sandy area called Landeyjarsandur. Data was saved on the instrument, but not collected remotely.

2.6.5 Reitur (IMO)

In the period 2 June to 6 July 2014 the OPC was measuring outside of the IMO on the measurements field called "Reitur" and again in August same year. Since 8 October 2014 the OPC has been measuring at the top of the roof at the IMO building.

2.6.6 Holuhraun

During the eruption in Holuhraun one OPC was installed close to the eruption site (N64.915365, W16.743812). The goal was to measure volcanic aerosols directly emitted by the fissure eruption or fine particles formed directly within the eruption plume. The OPC was measuring from 1 September-4 September 2014 and taken down because of lack of battery. It was set up again the 19 September with higher capacity battery connected to a solar panel and measured until 6 October 2014. Data were collected remotely.
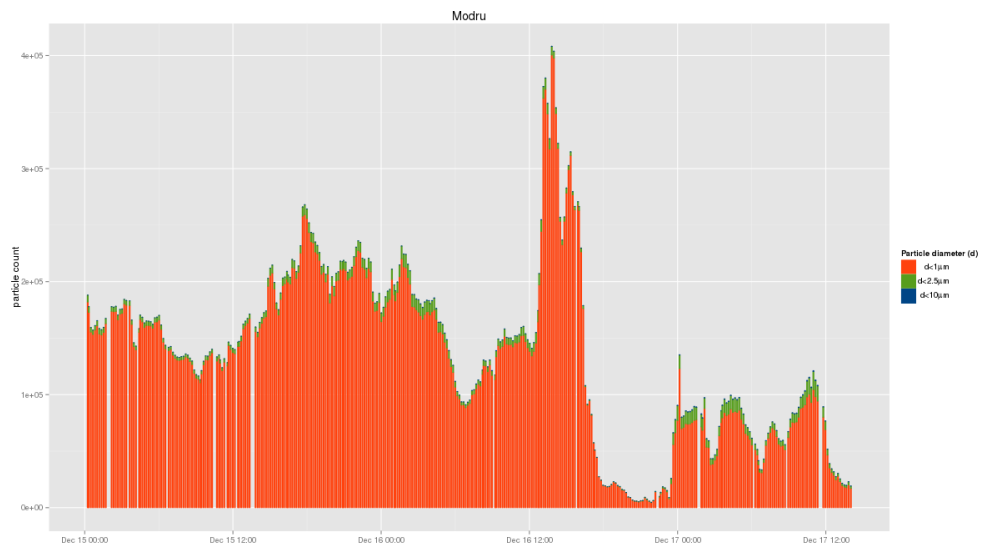
Figure 10: Two days' time series from the automatic script, data from Möðrudalur. Amount of counted particles are plotted against time. d=diameter, red columns represent particles with diameter smaller than 1 μm, green are particles with diameter smaller than 2.5 μm and blue are diameter smaller than 10 μm.

2.6.7 Möðrudalur

The farm Möðrudalur is in north-eastern Iceland 70 km NE of the eruption site in Holuhraun. As in Holuhraun the Möðrudalur OPC measurements have the aim to measure volcanic aerosols. Data are collected remotely since 12 September 2014.

2.7 Preliminary Results

In the real time data analysis raw data are presented as total particle counts vs. time (Fig. 10) where particle size is differentiated by < 1 μm (red), < 2.5 μm (green) and < 10 μm (blue) and as particle concentration vs. time (Fig. 11). From the plots it can be seen if there are increased number of airborne particles and it is in process to make a thresholds to alarm when sudden thresholds are received.

2.8 Conclusion

Since the start of the FutureVolc project, we were able to observe several dust storm events with the OPCs at different locations in Iceland. A data streaming and automated data processing tool have been developed during this project. Because the data set is still very small we are not be able to distinguish between aged volcanic ash and sand yet. There are also no data available for newly emitted volcanic ash. During the eruption in Holuhraun we were able to measure airborne particles directly emitted by the fissure or build within the eruption plume. A first analysis of these data has shown that there is a clear difference to the particle size distribution measured during a dust storm.

2.9 Outlook

The instruments are operational and can be installed within a short notice during a volcanic crisis. During the next weeks and months the focus will be on the analysis of the Holuhraun data as well as events in Möðrudalur and Svartárkot. Events with high number of particles will be looked at in detail (grain size distribution) and data-sets compared. At the end an alarm threshold for particle concentration will be set as well.
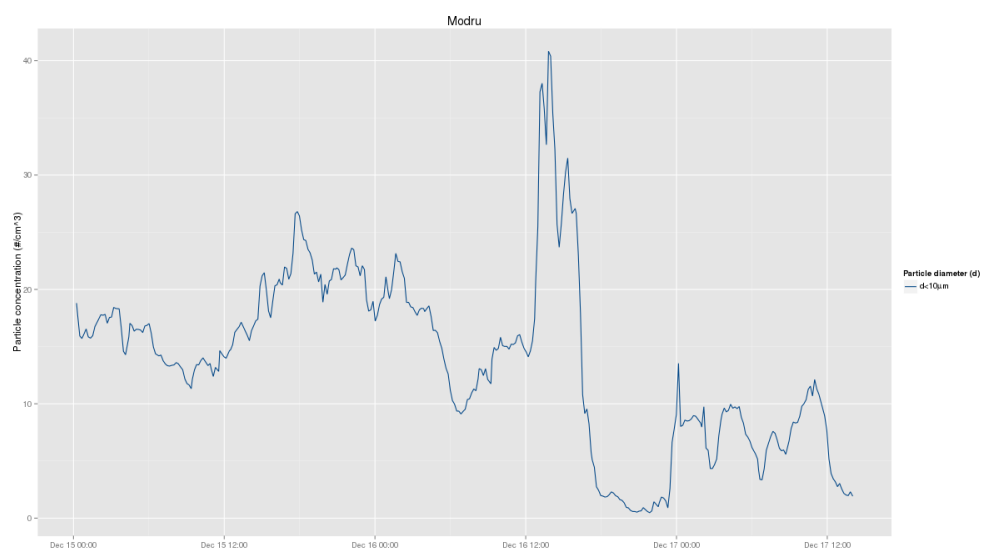
Figure 11: Two days' time series from the automatic script, data from Möðrudalur. Particle number concentration (#/cm^3) plotted against time.

Appendix A   The IRoPLUM software package

IRoPLUM consists of several python scripts which are briefly descrbied below.

To construct a synthetic target image, calculate line integrals for cameras viewing the target, reconstruct the image from the line integrals and compare the target and reconstructed images, the following scripts are available in IRoPLUM.

1. `SyntheticLineIntegrals.py` is used to generate synthetic targets and calculate the line integrals for one or more cameras viewing the targets. For each camera `SyntheticLineIntegrals.py` outputs a file containing the camera name, camera location and viewing geometry, and the line integral. Also the target image is stored to a file. `SyntheticLineIntegrals.py` was used to produce Figs. 2 and 3.

2. `Reconstruction2D.py` is used to reconstruct the target using the line integrals and camera geometry from the previous step. Output is to file.

3. `Compare.py` is used to compare the reconstructed image from `Reconstruction2D.py` and the "real" target image generated by `SyntheticLineIntegrals.py`.

4. `Tests.py` is used to run some simple tests of `SyntheticLineIntegrals.py` and `Reconstruction2D.py`.

The IRoPLUM software package includes the following directories:

- **bin** contains the python scripts mentioned above.

- **Examples** contains input and output files used to produce the results in Figs. 2, 3, 4, and 6. For reconstruction and plot of the density field in Fig. 4 the following commands were issued:

```
python Reconstruction2D.py
  —CameraFiles=../Examples/LineIntegralGauss_5Cameras_201RaysCam[1,2,3].dat
  —RRImageFile=../Examples/ImageFileGauss_3Cameras_201Rays
  —TargetImageFile=../Examples/TargetImageGauss_5Cameras_201Rays.pkl

python Compare.py
  —RRImageFile=../Examples/ImageFileGauss_3Cameras_201Rays
   —TargetImageFile=../Examples/TargetImageGauss_5Cameras_201Rays.pkl
```

  To reconstruct the density field in Fig. 6 and compare the reconstructed density field with the "real" density field the following commands were used:

```
python Reconstruction2D.py
  —CameraFiles=../Examples/LineIntegralGauss_5Cameras_201RaysCam?.dat
  —RRImageFile=../Examples/ImageFileGauss_5Cameras_201Rays
  —TargetImageFile=../Examples/TargetImageGauss_5Cameras_201Rays.pkl

 python Compare.py
  —RRImageFile=../Examples/ImageFileGauss_5Cameras_201Rays
  —TargetImageFile=../Examples/TargetImageGauss_5Cameras_201Rays.pkl
```

- **Tests** contains various input and output files used for running and checking the output from `bin/Tests.py`.

References

A. C. Kak and Malcolm Slaney: Principles of Computerized Tomographic Imaging, URL http://www.slaney.org/pct/, 2001.

Andersen, A. H. and Kak, A. C.: Simultanoues algebraic reconstruction technique (SART): A superior implementation of the ART algorithm, Ultrasonic Imaging, 6, 81–94, 1984.

Arnalds, O., Thorarinsdottir, E., Metusalemsson, S., Jonsson, A., Gretarsson, E., and Arnason, A.: Soil erosion in Iceland, The Soil Conservation Service, The Agricultural Research Institute, 2001.

Beister, M., Kolditz, D., and Kalender, W. A.: Iterative reconstruction methods in X-ray {CT}, Physica Medica, 28, 94 – 108, doi:http://dx.doi.org/10.1016/j.ejmp.2012.01.003, URL http://www.sciencedirect.com/science/article/pii/S112017971200004X, 2012.

Bender, R., Bellman, S. H., and Gordon, R.: ART and Ribosome: A preliminary report on the three-dimensional structure of individual ribosomes determined by and algebraic reconstruction technique, J. Theor. Biol., 29, 483–487, 1970.

Bruyant, P. P.: Analytic and iterative reconstruction algorithms in SPECT, J. Nucl. Med., 43, 1343–1358, 2002.

Dagsson-Waldhauserova, P., Arnalds, O., Olafsson, H., Skrabalova, L., Sigurdardottir, G., Branis, M., Hladil, J., Skala, R., Navratil, T., Chadimova, L., von Lowis of Menar, S., Thorsteinsson, T., Carlsen, H., and Jonsdottir, I.: Physical properties of suspended dust during moist and low-wind conditions in Iceland, Icelandic Agric. Sci., 27, 25–39, 2014.

Francis, P. N., Cooke, M. C., and Saunders, R. W.: Retrieval of physical properties of volcanic ash using Meteosat: A case study from the 2010 Eyjafjallajökull eruption, Journal of Geophysical Research: Atmospheres, 117, doi:10.1029/2011JD016788, URL http://dx.doi.org/10.1029/2011JD016788, 2012.

Gilbert, P.: Iterative methods for the three-dimensional reconstruction of an object from projections, J. Theor. Biol., 36, 105–117, 1972.

Gordon, R., Bender, R., and Herman, G. T.: Algebraic reconstruction techniques (ART) for three-dimensional electron microscopy and X-ray photography, J. Theor. Biol., 29, 471–481, 1970.

Hartl, A., Song, B. C., and Pundt, I.: 2-D reconstruction of atmospheric concentration peaks from horizontal long path DOAS tomographic measurements: parametrisation and geometry within a discrete approach, Atmospheric Chemistry and Physics, 6, 847–861, doi:10.5194/acp-6-847-2006, URL http://www.atmos-chem-phys.net/6/847/2006/, 2006.

Hinds, W. C.: Aerosol technology: properties, behavior, and measurement of airborne particles, 2nd ed., 1999.

Johansson, M., Galle, B., Rivera, C., and Zhang, Y.: Tomographic reconstruction of gas plumes using scanning DOAS, Bull Volcanol, 71, 1169–1178, 2009.

Kazahaya, R., Mori, T., Kazahaya, K., and Hirabayashi, J.-i.: Computed tomography reconstruction of SO2 concentration distribution in the volcanic plume of Miyakejima, Japan, by airborne traverse technique using three UV spectrometers, Geophysical Research Letters, 35, n/a–n/a, doi:10.1029/2008GL034177, URL http://dx.doi.org/10.1029/2008GL034177, 2008.

Laepple, T., Knab, V., Mettendorf, K.-U., and Pundt, I.: Longpath DOAS tomography on a motorway exhaust gas plume: numerical studies and application to data from the BAB II campaign, Atmospheric Chemistry and Physics, 4, 1323–1342, doi:10.5194/acp-4-1323-2004, URL http://www.atmos-chem-phys.net/4/1323/2004/, 2004.

Model 3330 Optical Particle Sizer Spectrometer: Operation and Service Manual, TSI., 2001.

Prata, A. J. and Bernardo, C.: Retrieval of volcanic ash particle size, mass and optical depth from a ground-based thermal infrared camera, Journal of Volcanology and Geothermal Research, 186, 91–107, 2009.

Prata, A. J. and Bernardo, C.: Retrieval of sulfur dioxide from a ground-based thermal infrared imaging camera, Atmospheric Measurement Techniques, 7, 2807–2828, doi:10.5194/amt-7-2807-2014, URL http://www.atmos-meas-tech.net/7/2807/2014/, 2014.

Price, P. N., Fischer, M. L., Gadgil, A. J., and Sextro, R. G.: An algorithm for real-time tomography of gas concentrations, using prior information about spatial derivatives, Atmospheric Environment, 35, 2827–2835, 2001.

Todd, L. A. and Bhattacharyya, R.: Tomographic reconstruction of air pollutants: evaluation of measurement geometries, Appl. Opt., 36, 7678–7688, doi:10.1364/AO.36.007678, URL http://ao.osa.org/abstract.cfm?URI=ao-36-30-7678, 1997.

Wang, G., Yu, H., and De Man, B.: An outlook on x-ray CT research and development, Medical Physics, 35, 1051–1064, doi:http://dx.doi.org/10.1118/1.2836950, URL http://scitation.aip.org/content/aapm/journal/medphys/35/3/10.1118/1.2836950, 2008.

Willemink, M., de Jong, P., Leiner, T., de Heer, L., Nievelstein, R., Budde, R., and Schilham, A.: Iterative reconstruction techniques for computed tomography Part 1: Technical principles, European Radiology, 23, 1623–1631, doi:10.1007/s00330-012-2765-y, URL http://dx.doi.org/10.1007/s00330-012-2765-y, 2013.

Wright, T. E., Burton, M., Pyle, D. M., and Caltabiano, T.: Scanning tomography of SO2 distribution in a volcanic gas plume, Geophysical Research Letters, 35, n/a–n/a, doi:10.1029/2008GL034640, URL http://dx.doi.org/10.1029/2008GL034640, 2008.

Zeng, G.: Image reconstruction - a tutorial, Computerized Medical Imaging and Graphics, 25, 97 – 103, doi:http://dx.doi.org/10.1016/S0895-6111(00)00059-8, URL http://www.sciencedirect.com/science/article/pii/S0895611100000598, 2001.